

EFFECT OF A HIGH OPACITY ON THE LIGHT CURVES OF RADIOACTIVELY POWERED TRANSIENTS FROM COMPACT OBJECT MERGERS

JENNIFER BARNES^{1,2}, DANIEL KASEN^{1,2}

(Received; Accepted)

Draft version August 21, 2018

ABSTRACT

The coalescence of compact objects are a promising astrophysical sources of gravitational wave (GW) signals. The ejection of r -process material from such mergers may lead to a radioactively-powered electromagnetic counterpart which, if discovered, would enhance the science return of a GW detection. As very little is known about the optical properties of heavy r -process elements, previous light curve models have adopted opacities similar to those of iron group elements. Here we report that the presence of heavier elements, particularly the lanthanides, increase the ejecta opacity by several orders of magnitude. We include these higher opacities in time dependent, multi-wavelength radiative transport calculations to predict the broadband light curves of one-dimensional models over a range of parameters (ejecta masses $\sim 10^{-3} - 10^{-1} M_{\odot}$ and velocities $\sim 0.1 - 0.3 c$). We find that the higher opacities lead to much longer duration light curves which can last a week or more. The emission is shifted toward the infrared bands due to strong optical line blanketing, and the colors at later times are representative of a blackbody near the recombination temperature of the lanthanides ($T \sim 2500$ K). We further consider the case in which a second mass outflow, composed of ^{56}Ni , is ejected from a disk wind, and show that the net result is a distinctive two component spectral energy distribution, with a bright optical peak due to ^{56}Ni and an infrared peak due to r -process ejecta. We briefly consider the prospects for detection and identification of these transients.

Subject headings: radiative transfer – supernovae

1. INTRODUCTION

A deeper understanding of compact object binary mergers has the potential to shed light on several important and unresolved questions in astrophysics. Binary neutron star mergers (NSMs) may be the central engines of short-duration gamma ray bursts (Paczynski 1986; Narayan et al. 1992), and heavy element nucleosynthesis in merger ejecta undergoing decompression from nuclear densities (Lattimer & Schramm 1974, 1976) may contribute to the production of r -process elements in the Universe (e.g. Eichler et al. 1989; Rosswog et al. 1998; Freiburghaus et al. 1999; Rosswog et al. 2000; Rosswog 2005; Goriely et al. 2005). With the LIGO (Abramovici et al. 1992) and VIRGO experiments preparing to upgrade to advanced status, compact object mergers provide the most likely source of kHz gravitational waves (GWs). The science returns from detected GW signals can be enhanced by the identification of a coincident electromagnetic signature (e.g. Schutz 1986, 2002; Stubbs 2008; Bloom et al. 2009).

Metzger & Berger (2012) consider several possible EM transients associated with compact object mergers – short-duration gamma ray bursts, orphan radio and optical afterglows, and optical “kilonovae” light curves – and conclude that the last of these offers perhaps the best opportunity for localizing GW signals. The kilonovae are optical transients powered by the radioactive decay of material ejected in the merger. Simulations suggest that somewhere in the range of $10^{-4} - 10^{-1} M_{\odot}$ may

be ejected either by tidal stripping during the merger itself, or later by a disk wind driven in the evolution of a post-merger remnant. The tidally ejected material is very neutron rich and should form heavy elements via the r -process, while the subsequent outflows are probably less neutron rich and nucleosynthesis may not extend much beyond the iron peak. In either case, the brightness of the resulting light curves will be set by the mass of radioisotopes ejected, while the duration depends on the effective diffusion time through the ejecta, and hence on the mass, velocities, and opacities. While the nucleosynthesis and radioactive heating has been modeled with a fair degree of detail (Metzger et al. 2010; Roberts et al. 2011; Goriely et al. 2011), the unknown opacities of r -process elements have posed a major challenge to predicting kilonova light curves and spectra.

Li & Paczyński (1998) were the first to study the r -process transients from NSM. Their simplified one-zone model assumed spherical symmetry and a blackbody spectrum, and absorbed much of the physical complexity of the system into a set of input parameters. Assuming opacities on the order of the electron scattering opacity, they predicted that the light curves would peak in the optical/ultraviolet and rise to peak bolometric luminosities of $10^{42} - 10^{44}$ ergs s^{-1} on a timescale of a day. More recent, more detailed, models (Metzger et al. 2010; Roberts et al. 2011) have used nuclear reaction networks to determine the radioactive heating rate and Monte Carlo radiation transport to calculate merger light curves, under the assumption that the opacities of heavy r -process elements could be approximated by those of iron. These newer models found qualitatively similar results, with peak bolometric luminosities $\sim 10^{41} - 10^{42.5}$ ergs s^{-1} and rise times around

¹ Departments of Physics and Astronomy, 366 LeConte Hall, University of California, Berkeley, CA, 94720

² Nuclear Science Division, Lawrence Berkeley National Laboratory, Berkeley, CA 94720

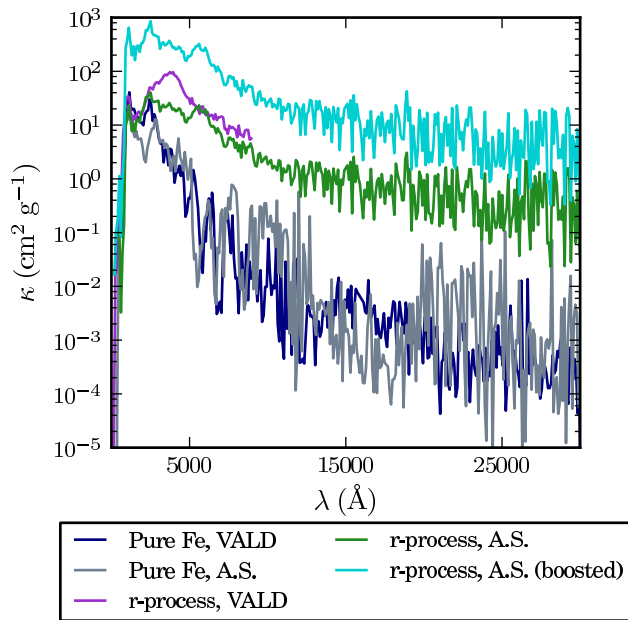


FIG. 1.— Wavelength dependent expansion opacities for ejecta with $\rho = 10^{-13} \text{ g cm}^{-3}$, $T = 5000 \text{ K}$, and $t_{\text{exp}} = 1 \text{ day}$. The opacity of iron is calculated using both the VALD and `Autostructure` line lists to demonstrate the reliability of the latter approach. The r -process opacity calculated using `Autostructure` data for Nd is in fairly good agreement with that using the VALD line list (which only includes extensive line data for a few heavy elements). The *boosted* r -process opacity takes into account the diversity of species in an r -process mixture by assuming that all lanthanides have an opacity comparable to Nd.

one day, with the colors rapidly reddening post-peak.

In this paper, we show that using more realistic opacities of r -process material has a dramatic effect on the predicted kilonova light curves. We use improved estimates of the atomic data of heavy elements derived from *ab initio* atomic structure models (Kasen et al. 2013, hereafter K13). The r -process opacities we find are orders of magnitudes higher than the those of iron group elements; as a consequence, we predict light curves that are longer, dimmer, and redder than previously thought. Rather than peaking sharply at $t \simeq 1 \text{ day}$, the duration of the bolometric light curves can last $\sim 1 \text{ week}$. The spectral energy distribution (SED) is highly suppressed in the optical, with the bulk of the energy emitted in the infrared. Such findings can inform observational searches for an EM counterpart to a GW trigger by clarifying the transient timescales, the bands in which EM emission will be strongest (or have the most distinct signature), and the distances out to which we might expect a successful EM detection.

2. OPACITY OF R-PROCESS EJECTA

Supernova calculations suggest that for complex ions (e.g., the iron group) bound-bound transitions dominate other forms of opacity, such as electron scattering, free-free, and photoionization (e.g. Pinto & Eastman 2000). Literally millions of lines, Doppler-broadened by the remnant’s differential velocities, will contribute to a pseudo-continuum bound-bound opacity. Photons trav-

eling through the ejecta are continually Doppler-shifted with respect to the comoving frame, and come into resonance with multiple transitions one by one. The velocity gradient of the remnant thus enhances the effective line opacity (Karp et al. 1977). We account for this effect using the expansion opacity formalism introduced by Karp et al. (1977) and further developed by Eastman & Pinto (1993), where the extinction coefficient is given by

$$\alpha_{\text{exp}}(\lambda_c) = \frac{1}{ct_{\text{exp}}} \sum_i \frac{\lambda_i}{\Delta\lambda_c} (1 - e^{-\tau_i}). \quad (1)$$

This formula represents an average over discrete wavelength bins, where t_{exp} is the time since mass ejection, λ_c is the central wavelength of the bin, $\Delta\lambda_c$ is the bin width, τ_i is the Sobolev optical depth of a line (Sobolev 1960), and the sum runs over all lines in the bin. The extinction coefficient is related to the expansion opacity by $\kappa_{\text{exp}} = \alpha_{\text{exp}}/\rho$, where ρ is the gas density.

To calculate Sobolev line optical depths, we assume that the atomic level populations are set by local thermodynamic equilibrium (LTE). This approximation should be reasonable in the optically thick regions of ejecta, where the radiation field tends towards a blackbody distribution. In applying the a Sobolev formalism, we make two further assumptions: first, that the intrinsic (Doppler) width of lines is small compared to the velocity scale over which the ejecta properties vary, and second, that the intrinsic profiles of strong lines do not overlap with other lines. While the first condition is easily satisfied in rapidly expanding NSM ejecta, the second may not be (see K13), and a non-Sobolev treatment may ultimately be necessary for a fully rigorous treatment of the radiation transport.

The expansion opacity takes a simplified form in atmospheres where most lines are extremely optically thick ($\tau \gg 1$). As τ_i increases, the dependence of α_{exp} on optical depth is eliminated ($1 - e^{-\tau_i} \simeq 1$), and the expression for expansion opacity simplifies to a sum of optically thick lines. The dependence on density and other determinants of optical depth are concomitantly reduced. Under these conditions, the number of distinct optically thick lines in each bin becomes the most important predictor of ejecta opacity. An exhaustive tally of lines is therefore essential to accurately modeling ejecta opacity. Unfortunately, there is relatively little line data available for the heavy elements ($Z > 28$) expected to be synthesized in NSM ejecta. We compiled the line data provided in the VALD database (Heiter et al. 2008), which includes fairly extensive data for a few heavy ions (e.g. CeII, CeIII), but very little for most others species.

On theoretical grounds, we expect the lanthanides (atomic numbers $Z = 58 - 72$) to contribute significantly to ejecta opacity, due to the complicated structure of their valence f-shells. This argument is illustrated with a simple combinatorics heuristic. The number of substates corresponding to a given electron orbital is roughly

$$C = \frac{g!}{n!(g-n)!} \quad \text{with } g = 2(2l+1), \quad (2)$$

where n is the number of valence electrons and l is the angular momentum quantum number of the valence shell. The number of lines should scale as C^2 , and will be much

greater for ions with electrons in an open f ($l = 3$) shell. Assuming lines from the two species are equally likely to be optically thick, we expect atmospheres containing lanthanides to have a much higher opacity than atmospheres of pure iron. A similar argument could be applied to elements of the actinide series, which may also be produced in the merger ejecta. However, the mass fractions of most actinides are predicted to be low, and can likely be ignored.

Initial calculations of opacities using line data from VALD suggested that lanthanides have a much higher expansion opacity than iron (see Figure 1). However, the limited line data available in the VALD database makes it difficult to predict opacities over a range of ionization states. Instead, we use the theoretical lanthanide line data of K13 derived from the atomic structure modeling code `Autostructure` (Badnell 2011). This supplies approximate radiative data for neodymium ($Z = 60$) and a few other elements over the entire wavelength range of interest ($\sim 100 \text{ \AA} - 30,000 \text{ \AA}$). We tested the reliability of the `Autostructure` data by comparing predicted expansion opacities of select species, including Fe and Ce, to those calculated using existing line data in VALD. Overall, the results from both data sets are found to be in good agreement (Figure 1).

Until `Autostructure` models for all lanthanides are calculated, we use an averaging scheme to predict ejecta opacities based on a few representative species. We recast the ejecta composition computed by Roberts et al. (2011) in terms of two groups of elements: iron-like elements (i.e., the d-block of the periodic table) and neodymium-like elements (i.e., the lanthanides). The line data for iron is taken from Kurucz & Bell (1995), while that of Nd is derived from `Autostructure` calculations. We take the mass fraction of Nd (Fe) to be equal to the average mass fraction of the lanthanides (d-block elements). The remainder of the composition is taken to be calcium, which serves as a low-opacity filler with an appropriate ionization potential.

Since each ion species in the ejecta has a unique set of strong lines, and since α_{exp} increases with the number of strong lines, mixtures with a greater diversity of elements will have higher opacity. Since both Nd and Fe both have intermediate complexity for their respective blocks, their opacities can presumably be taken as representative of other elements in the same region of the period table. We therefore assume that each lanthanide or d-block element in the original compositions provides an opacity equal to that of Nd or Fe, respectively, and arrive at a generalized expression for expansion opacity

$$\alpha_{\text{exp}} = \frac{1}{ct_{\text{exp}}} \sum_Z N_Z \sum_i \frac{\lambda_i}{\Delta\lambda_c} \left(1 - e^{-\tau_i(\rho_Z)}\right), \quad (3)$$

where Z runs over the representative elements (here Fe and Nd), N_Z is the number of elements in the block represented by Z , and $\rho_Z = \chi_Z \rho$, with χ_Z the mean mass fraction of the representative elements. Since lanthanide contributions dominate the opacity, the boosting procedure effectively increases the opacity by a factor of 14, the number of lanthanide species.

Figure 1 shows the expansion opacity calculated for typical parameters of NSM ejecta ($\rho = 10^{-13} \text{ g cm}^{-3}$, $T = 5 \times 10^3 \text{ K}$, and $t_{\text{exp}} = 1 \text{ day}$). The

values vary with temperature and density, but in general our calculations predict r -process opacities many orders of magnitude higher than those calculated for iron group elements.

3. LIGHT CURVES OF R -PROCESS TRANSIENTS

The surprisingly high opacity of r -process material, discussed in §2, has important implications for the EM emission from NSMs. In this section, we present radiation transport calculations using our refined opacity estimates to determine the bolometric and broadband light curves of r -process outflows. Our predictions diverge from those of earlier studies, which assumed that the opacities were similar to those of iron.

3.1. Ejecta Model

We model the NSM ejecta as a spherically symmetric outflow undergoing homologous expansion. In reality, the ejecta may have a highly asymmetric, ‘‘tidal tail’’ geometry (Rosswog 2005). 3-D transport calculations suggest that this asphericity makes the emission moderately anisotropic, but does not qualitatively change the shape of the light curves (Roberts et al. 2011). We describe the density of the ejecta using the broken power law profile introduced by Chevalier & Soker (1989), in which density decreases as $r^{-\delta}$ in the inner layers of the atmosphere and as r^{-n} (with $n > \delta$) in the outer layers. The shift from n to δ occurs at the transition velocity

$$v_t = 7.1 \times 10^8 \zeta_v (E_{51}/M)^{1/2} \text{ cm s}^{-1}, \quad (4)$$

where E_{51} is the explosion energy $E/10^{51}$ ergs, M is the ejecta mass M_{ej} in units of M_{\odot} , and ζ_v is a numerical constant. For $v < v_t$, the density is given by

$$\rho(r, t) = \zeta_{\rho} \frac{M_{\text{ej}}}{v_t^3 t^3} \left(\frac{r}{v_t t}\right)^{-\delta}, \quad (5)$$

and an analogous expression describes the outer layers. The constants ζ_v and ζ_{ρ} satisfy the requirement that the density profile integrates to the specified mass and energy. We also tried using an exponentially decreasing density profile, but found that the light curves were mostly insensitive to the details of the density structure. The results presented here were generated using the broken power law profile with $(n, \delta) = (1, 10)$.

The mass and velocities of the matter ejected during compact object mergers is still uncertain. Simulations of NSMs (e.g. Rosswog et al. 1999; Oechslin et al. 2007; Goriely et al. 2011; Hotokezaka et al. 2013) and of neutron star-black hole mergers (e.g. Janka et al. 1999; Lee 2001; Rosswog 2005) have found that the amount of material ejected is sensitive to binary type, mass ratio, nuclear equation of state, and the treatment of gravity (Newtonian v. general relativistic). However, taken in aggregate, simulations suggest NSMs may eject $\sim 10^{-2} M_{\odot}$ of material with velocities on the order of $\beta = v/c \sim 0.1$. We adopt these parameters as our fiducial model, but vary the mass and velocity scales over the range $M = 10^{-3} - 10^{-1} M_{\odot}$, and $\beta_{\text{char}} = 0.1 - 0.3$, where we define the characteristic velocity by

$$E = \frac{1}{2} M_{\text{ej}} (\beta_{\text{char}} c)^2. \quad (6)$$

TABLE 1
PEAK MAGNITUDES AND BOLOMETRIC LIGHT CURVE PROPERTIES OF RADIOACTIVE TRANSIENTS

$M_{\text{ej}} (M_{\odot})$	β	composition	$L_{\text{p,bol}}^{\text{a}}$	$t_{\text{p,bol}}^{\text{b}}$	M_B	M_R	M_I	M_H
10^{-3}	0.1	r-proc	1.2×10^{40}	0.65	-9.3	-11.2	-12.0	-14.0
10^{-3}	0.2	r-proc	1.6×10^{40}	0.75	-9.1	-11.3	-12.6	-14.1
10^{-3}	0.3	r-proc	3.5×10^{40}	0.15	-9.3	-12.4	-13.6	-14.7
10^{-2}	0.1	r-proc	5.2×10^{40}	4.25	-11.2	-12.7	-13.3	-15.8
10^{-2}	0.2	r-proc	8.5×10^{40}	1.85	-11.4	-12.8	-14.0	-15.9
10^{-2}	0.3	r-proc	1.7×10^{41}	0.25	-11.8	-14.1	-15.2	-16.5
10^{-1}	0.1	r-proc	2.4×10^{41}	8.65	-12.9	-14.1	-14.6	-17.5
10^{-1}	0.2	r-proc	4.1×10^{41}	4.35	-13.4	-14.3	-15.4	-17.5
10^{-1}	0.3	r-proc	7.2×10^{41}	0.25	-14.0	-15.5	-16.7	-18.1
10^{-3}	0.1	^{56}Ni	3.5×10^{40}	0.25	-13.0	-12.6	-12.6	-11.8
10^{-2}	0.1	^{56}Ni	3.7×10^{41}	0.75	-15.4	-14.9	-14.5	-14.8

^aPeak bolometric luminosity, in ergs s^{-1}

^bRise time to bolometric light curve peak, in days

We assume the ejecta to be homogenous, and composed of either pure r -process material or pure ^{56}Ni . For models with r -process elements, all zones are assumed to have the same radioactive decay rate given by Roberts et al. (2011). Of the decay energy, 10% is taken to be in fission fragments, and 90% in beta decays. Of the beta decay energy, 75% is assumed to be lost to neutrinos, with the remaining 25% split equally between leptons and gamma-rays. Leptons and fission fragments are assumed to be thermalized locally, while we use a radiation transport scheme to follow the propagation and absorption of gamma rays. This approximate apportioning of the decay energy is based on the physical considerations given in Metzger et al. (2010).

3.2. Light Curves

We generate synthetic observables of our ejecta models using the time-dependent multi-wavelength radiation transport code *Sedona* (Kasen et al. 2006). Beginning at an initial time of 0.1 days after mass ejection, the code follows the temperature and density evolution of the expanding ejecta, taking into account radiative and radioactive heating as well as cooling by expansion. The wavelength dependent r -process and iron opacities are calculated in each zone using the *Autostructure* and Kurucz & Bell (1995) line data, respectively. The ionization and excitation state of the gas are assumed to be set by LTE, and lines are taken to be completely absorbing. *Sedona* synthesizes the emergent spectral time series, from which we construct bolometric and broadband light curves. Table 1 summarizes the EM properties of the models we investigated.

In Figure 2, we plot the bolometric light curves of r -process transients for a subset of the parameter grid. For comparison, we also show a light curve calculated using iron-like opacities. Introducing more realistic r -process opacities clearly changes the picture significantly – the light curves have slower rise times and broader, dimmer peaks than those calculated with iron-like opacities. Notably, the r -process transients do not in general have the ~ 1 day duration thought to be a distinguishing feature of these events, and instead may last a week or longer.

That higher opacities give broader, dimmer light curves is expected theoretically. The duration of radioactively powered bolometric light curves is set by the effective

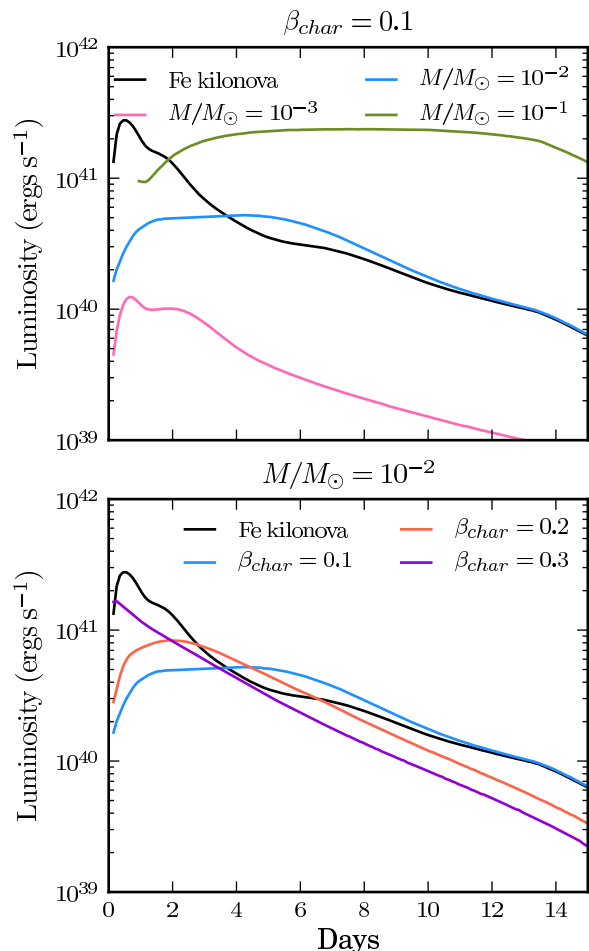


FIG. 2.— Synthetic bolometric light curves of r -process transients with different ejecta masses (top panel) and velocities (bottom panel). For comparison, we also show the light curve of a model with fiducial ejecta parameters ($M = 10^{-2} M_{\odot}$, $\beta_{\text{char}} = 0.1$) but calculated assuming iron-like opacities (black lines). The higher opacities of r -process ejecta lead to significantly broader light curves. The models with higher ejecta velocities correspond to shorter rise times and steeper declines, while those with higher masses have greater luminosities and longer durations.

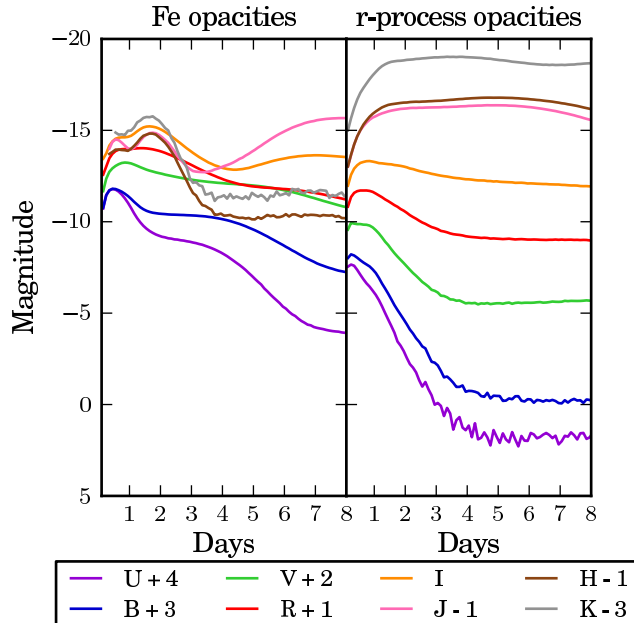


FIG. 3.— Synthetic broadband light curves calculated for the fiducial ejecta model calculated using iron-like opacities (left) and r -process opacities (right). The effect of r -process opacities is to suppress the optical emission and shift the radiation toward redder bands, in particular the infrared J, H and K bands.

tive diffusion time through the ejected material (Arnett 1979),

$$t_d \simeq \left(\frac{M_{\text{ej}} \kappa}{vc} \right)^{\frac{1}{2}}, \quad (7)$$

where v is a characteristic ejecta velocity and κ an appropriately wavelength-averaged opacity. Because the r -process opacities are 10 – 100 times larger than those of iron, the diffusion time is significantly lengthened. The longer diffusion time also leads to a dimmer luminosity at peak, as a greater fraction of the radioactive energy is lost due to expansion before it can be radiated. The models roughly obey Arnett’s law – i.e., the emergent luminosity and instantaneous radioactive energy input are approximately equal at peak (Arnett 1979, 1982).

The r -process light curves vary with the ejecta properties in predictable ways. Higher mass ejections give a greater luminosity and longer duration, due to their larger radioactive mass. Ejecta models with higher kinetic energies have shorter rise times, reach greater peak luminosities, and decline more rapidly than their lower energy analogues. Over the reasonable range of ejecta parameters considered here, the light curves exhibit significant diversity – the peak luminosities vary by more than an order of magnitude, and the durations range for $\lesssim 1$ day to as long as two weeks.

The broadband magnitudes of the models also differ significantly from previous expectations. Figure 3 shows that, compared to a model that uses iron-like opacities, r -process transients output much more energy in red and infrared bands, with a strong suppression of the optical emission. We find bright, broad peaks in the J, H, and K bands, while the U, B, and V bands are heavily line blanketed and decline sharply at early times. Figure 4 shows that the colors of the fiducial r -process model red-

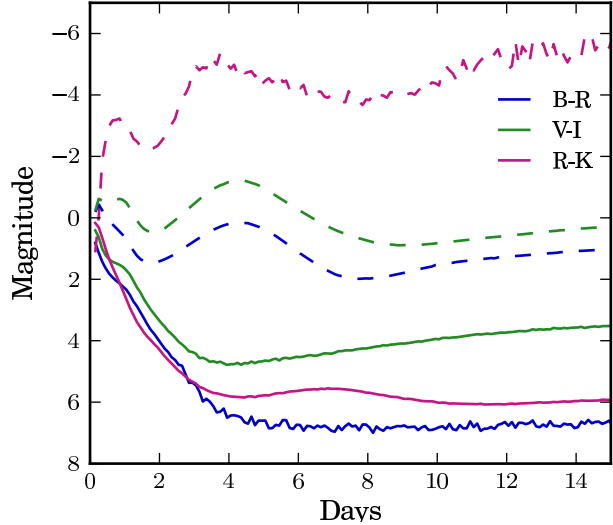


FIG. 4.— Select colors for the fiducial model calculated using r -process (solid lines) and iron-like (dashed lines) opacities. The colors of r -process transients initially redden rapidly, then reach a phase of constant color characterized by a blackbody at $T \approx 2500$ K.

den rapidly over the first day or two, and afterwards become remarkably constant, with the SED peaking in the infrared at around $\sim 1 \mu\text{m}$. Other than the very red color, the spectra at these phases resemble those of other high-velocity SNe, with a pseudo blackbody continuum and broad ($\sim 200 \text{ \AA}$) spectral features (see K13).

The behavior of the broadband light curves can be understood by examining the photospheric properties of r -process transients, since the observed SED roughly corresponds to a blackbody at the photospheric temperature and radius. In Figure 5, we plot the velocity and temperature evolution of the photosphere, the surface defined by

$$\tau(r_{\text{phot}}) = - \int_{\infty}^{r_{\text{phot}}} \bar{\kappa}_P(r) \rho(r) dr = 1, \quad (8)$$

where $\bar{\kappa}_P(r)$ is the Planck mean opacity, computed from our r -process line data.

In the initial phases, the photospheric velocity and temperature decline steadily, reflecting the decrease in density and cooling of the ejecta due to expansion. At around ~ 2 days, however, the photospheric temperature stabilizes at $T \simeq 2500$ K. Since this is close to the first ionization temperature of the lanthanides, this plateau probably reflects the sharp drop in opacity that occurs when these elements recombine to neutral (see K13). Recombination occurs in the cooler outer layers first, and a sharp ionization front forms in the ejecta. Photons pass easily through the cooler, neutral outer layers, but are trapped in the ionized inner regions – the photosphere thus forms at the ionization front. During this phase, the emergent colors are roughly constant in time and resemble those of a blackbody at the lanthanide recombination temperature. Over time, the recombination front recedes inward, reaching the center at around 14 days. At this point, the ejecta is nearly entirely neutral and transparent.

3.3. Uncertainties in the Opacities

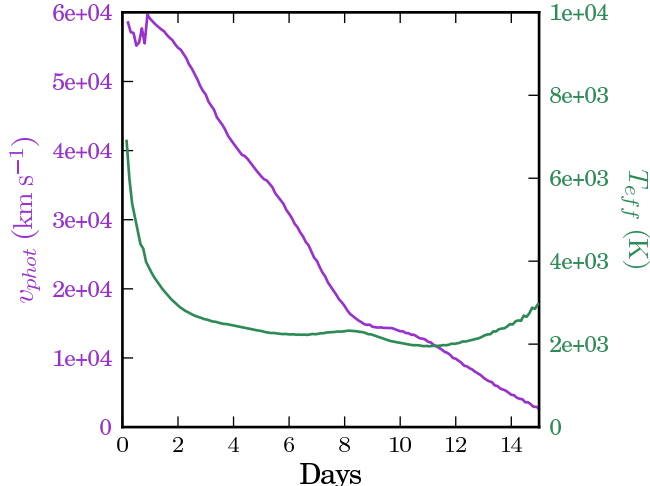


FIG. 5.— Evolution of the photospheric temperature and velocity in the fiducial model, using r -process opacities. The photospheric temperature initially declines rapidly, but at times $\gtrsim 2$ days settles to a fixed value near the recombination temperature of the lanthanides.

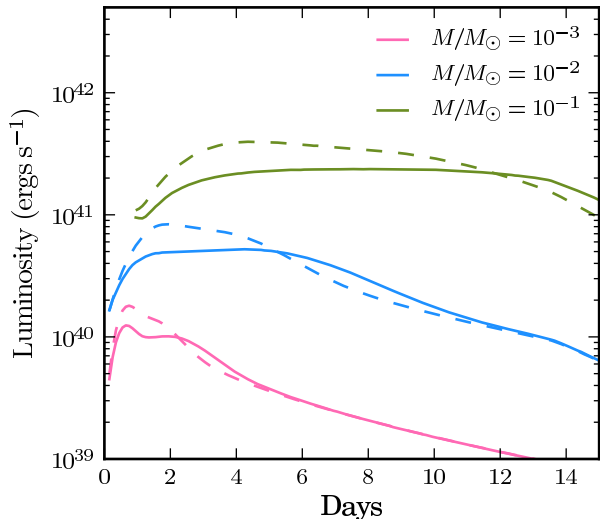


FIG. 6.— Bolometric light curves for $\beta_{\text{char}} = 0.1$ and a range of ejecta masses, calculated using line data with from two different **Autostructure** models of Nd, each with a somewhat different energy level structure. Solid curves correspond to our preferred **Autostructure** model (*opt3*), while dashed curves show results from an alternative model (*opt2*). The moderate differences can be taken as a rough estimate of the error resulting from uncertainties in the Nd structure models.

Though our r -process opacities represent an improvement over previously available data, the **Autostructure** models of Nd are subject to uncertainties. In particular, the structure models rely on an *ab-initio* optimization, such that the predicted atomic level energies and line wavelengths generally differ from the experimental values. To explore the effects of these uncertainties, we calculated bolometric and broadband light curves using two different **Autostructure** models of Nd (*opt2* and *opt3* from K13) each with a somewhat different energy level structure. The *opt3* model—which we have used in the calculations presented thus far—reproduces the low lying

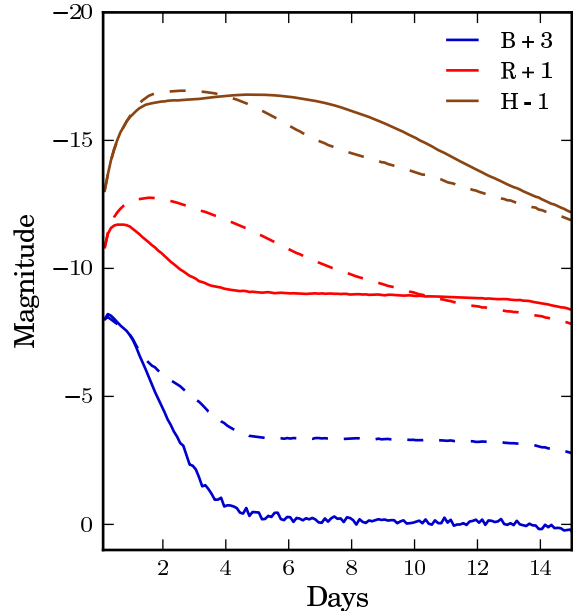


FIG. 7.— A comparison of broadband curves of the fiducial model, calculated using line data with from two different **Autostructure** models of Nd, each with a somewhat different energy level structure. Calculations using the *opt2* line data (dashed lines) predicts higher magnitudes for the optical B-, and R-bands than those with the *opt3* line data (solid lines)

energy levels of NdII quite well, while the *opt2* model has generally higher excitation energies which are harder to populate under our assumption of LTE. The result is fewer strong lines and a lower overall opacity for the *opt2* case.

In Figure 6, we plot bolometric light curves for ejecta models with $\beta_{\text{char}} = 0.1$ and a variety of masses. The light curves calculated using the *opt2* line data have somewhat sharper, more luminous peaks and swifter declines, consistent with the expected lower opacities. The differences, however, are fairly modest, and the bolometric luminosity never differs by more than a factor of ~ 3 . The effects are more noticeable in the broadband light curves (Figure 7). In particular, the R-band light curves are $\sim 1-2$ magnitudes brighter for the *opt2* data, which could have important implications for detectability. Based on comparison to experiment, we expect the *opt3* data to be more reliable, however further work refining the opacities is clearly warranted.

In addition to errors inherent in the individual structure models, a perhaps larger uncertainty in our r -process opacities arises from the fact that we represent all lanthanides with the radiative data of Nd. In fact, the lanthanides with a nearly half open f-shell (in particular gadolinium) will be significantly more complex, with perhaps ~ 10 times as many lines of Nd. We therefore suspect that our current calculations underestimate the true opacity. The light curves we present here suggest that increasing the opacity further will lead to an even greater suppression of optical emission.

3.4. A ^{56}Ni -powered transient

Given that the radioactive light curves of NSMs depend strongly on the composition of the ejecta, it is worth considering whether any elements lighter than the lan-

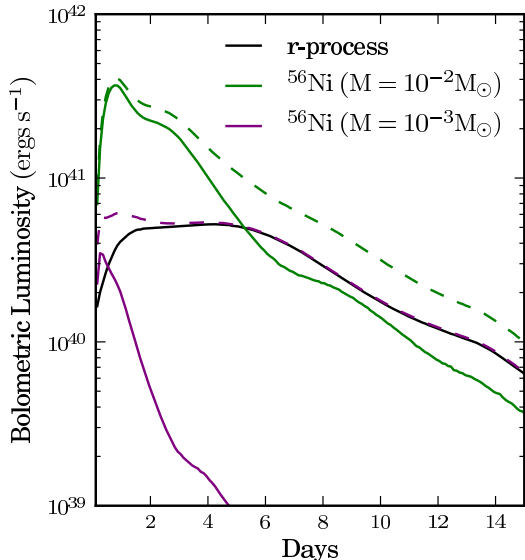


FIG. 8.— Bolometric light curves for models that include two components: r -process material (from tidal tails) and ^{56}Ni (from a disk wind). We plot the light curve of the fiducial r -process ejecta model ($M_{\text{rp}} = 10^{-2} M_{\odot}$, black line) along with two models of pure ^{56}Ni with different masses ($M_{\text{ni}} = 10^{-2} M_{\odot}$ and $10^{-3} M_{\odot}$, green and purple solid lines). The dashed lines give the combined two-component light curves.

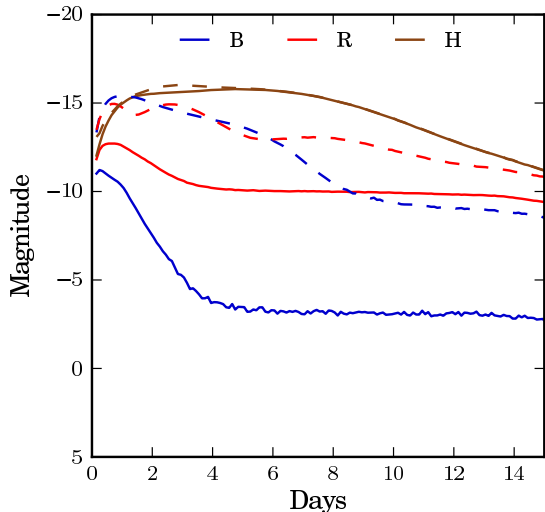


FIG. 9.— A comparison of select broadband light curves for a pure r -process transient (solid lines) and an r -process transient combined with a ^{56}Ni -powered outflow (dashed lines). The bluer SED from the ^{56}Ni shifts the magnitudes of the bluer bands of the combined SED upward relative to a pure r -process model. This plot is for $M_{\text{ni}} = M_{\text{rp}} = 10^{-2} M_{\odot}$.

thanides may be produced in these events. While the material dynamically ejected in the merger itself (the tidal tails) is thought to undergo robust r -process nucleosynthesis, it is plausible that a comparable amount of mass may subsequently be blown off in winds from an accretion disk surrounding the merged remnant. Though

the physical properties of the disk winds remain uncertain, neutrino irradiation may drive the electron fraction to $Y_e \gtrsim 0.4$, in which case the nucleosynthesis may not extend past $Z \sim 50$ (Surman et al. 2006, 2008; Metzger et al. 2008; Darbha et al. 2010). If Y_e is very close to 0.5, the composition will be primarily ^{56}Ni . In this case, the EM signature of a merger may be a superposition of a ^{56}Ni - and a r -process-powered transient.

To address this possibility, we consider a simplified scenario where $10^{-3} - 10^{-2} M_{\odot}$ of pure ^{56}Ni is blown off in a wind immediately post-merger. Consistent with our use of spherical symmetry thus far, we model this wind as a spherical outflow, with $\beta_{\text{char}} = 0.1$ and the same broken power law density profile with $(n, \delta) = (1, 10)$. We consider the tidal tails and disk wind to be two separate, non-interacting components, which is perhaps not unreasonable given that the winds are likely collimated in the polar regions, while the tidal tails are largely confined to the orbital plane. Ignoring viewing angle effects, we take the two component light curve to simply be the superposition of the individual ^{56}Ni -powered and the r -process powered light curves.

Figure 8 shows the two component light curves, for two different ratios of the ^{56}Ni wind mass (M_{ni}) to the r -process tidal tail mass (M_{rp}). For $M_{\text{ni}} \ll M_{\text{rp}}$, the primary effect of the ^{56}Ni wind is to raise the early-time luminosity, creating a very short peak at $t \sim 1$ day, which blends into the long, flat, r -process light curve. The cumulative light curve thus appears to have a faster rise time and longer plateau. If $M_{\text{ni}} \approx M_{\text{rp}}$, the ^{56}Ni emission dominates the r -process emission for the first ~ 5 days post merger, with the two components contributing roughly equally thereafter. The net effect is a gradually declining light curve, with the long r -process plateau obscured by the ^{56}Ni -powered light curve.

The addition of a ^{56}Ni component also affects the SED of the transient, as shown in Figure 9 for the case $M_{\text{ni}} = M_{\text{rp}} = 10^{-2} M_{\odot}$. Given the much lower iron group opacities, the SED of the ^{56}Ni ejecta is much bluer than that of the r -process ejecta. The emission in the optical bands (U,B,V,R) is relatively bright and set by ^{56}Ni mass, while the r -process material establishes the behavior in the infrared bands. Such an unusual SED may serve as an EM fingerprint that could improve the prospects for positively identifying a NSM. In particular, as shown in Figure 10, the spectrum of a two component outflow is, to first approximation, the superposition of two blackbodies – a sharply peaked bluer blackbody, corresponding to the ^{56}Ni ejecta, and a lower, redder one, corresponding to the r -process material.

The aggregate light curve model we present here glosses over some of the more complex physical processes. Our model assumes spatially distinct regions of pure ^{56}Ni and pure r -process material. In reality, the nucleosynthetic yields are highly sensitive to the conditions in the wind, and it is possible that disk outflows contain some elements heavier than ^{56}Ni . Contamination of the outflows with even a small mass fraction of lanthanides ($\sim 10^{-3}$) can significantly increase the opacities and the optical line blanketing. Even if our simplified compositions turn out to be reasonable, our model does not account for the geometry of the ejecta and any possible mixing of the wind and tidal tail components. Given

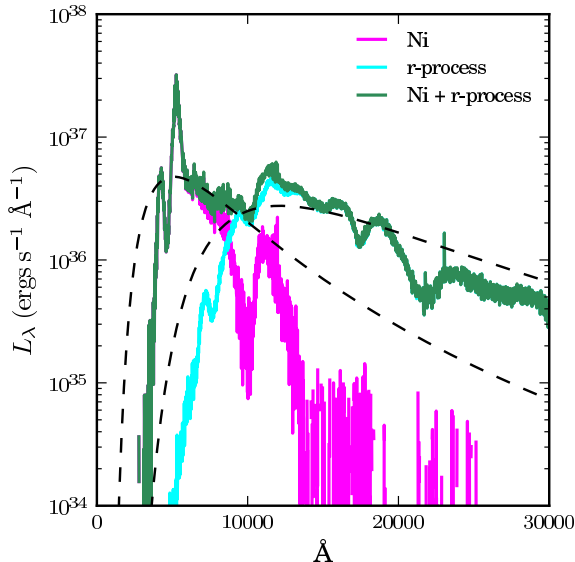


FIG. 10.— A combined ^{56}Ni and r -process spectrum at $t = 7$ days, taking $M_{\text{Ni}} = M_{\text{rp}} = 10^{-2} M_{\odot}$. The peak at blue wavelengths is due to the ^{56}Ni while the r -process material supplies the red and infrared emission. The best fit blackbody curves to the individual spectra are overplotted in dashed black lines ($T_{\text{Ni}} \simeq 5700$ K, $T_{\text{rp}} \simeq 2400$ K). The combined spectrum roughly resembles the superposition of two blackbodies at different temperatures.

the presumably high level of asymmetry, the net (tails + wind) EM output may depend heavily on orientation, making our simple superposition procedure valid only along certain lines of sight.

4. CONCLUSION

We have shown that the radioactive powered light curves associated with NSMs are greatly modified when more realistic values for the opacities of r -process material are taken into account. The r -process opacities are much higher than those of iron, due to both the complexity of heavy elements (in particular the lanthanides) and the diversity of atomic species present. Refining our understanding of the atomic structure of these elements is an important step toward a more rigorous model of transients from merging compact objects.

In accordance with theoretical expectations, the extremely high r -process opacities result in bolometric light curves that are broader and dimmer than those calculated assuming iron-like opacities. Our calculations indicate that the light curves are likely to last at least a few days, and may endure as long as a week or two in certain cases. The broadband magnitudes are also significantly impacted – we find heavy line blanketing in the optical and UV bands, with most of the radiation emitted in the near infrared. The colors at later times are fairly constant, and regulated to be similar to a blackbody at $T \approx 2500$ K, the recombination temperature of the lanthanides.

These findings have important, if mixed, consequences for the detectability of EM counterparts to NSMs. On the one hand, we predict dimmer bolometric luminosities and SEDs largely shifted into the infrared, both of which pose serious challenges to observational surveys at optical wavelengths. On the other hand, the light curves are

of longer duration, and may not require quite as a high cadence of observations. Perhaps more importantly, the uniquely high opacity of r -process ejecta provides signatures that may allow us to distinguish NSMs from other sorts of dim transients. In particular, the SED of r -process ejecta peaks in the infrared, with a color temperature set by lanthanide recombination. If the merger ejects two separate mass components – r -process tidal tails and a ^{56}Ni wind – the dual spectrum may be quite distinctive, with discernible infrared and optical components.

The SEDs we predict can be used to roughly estimate the detectability, given the varying depths and wavelength coverage of different observing facilities (e.g., Nissanke et al. 2012). For example, Pan-STARRS (see <http://pan-starrs.ifa.hawaii.edu>) and PTF (Law et al. 2009) achieve an R-band depth of $M_R \sim 21$ magnitudes, while LSST reaches a depth of $M_R \sim 24$ (LSST Science Collaborations 2009). We find that an r -process transient with fiducial model parameters will peak at $M_R = -13$, which under ideal observing conditions, would be observable to Pan-STARRS or PTF out to a distance of ~ 60 Mpc. This is an interesting, but rather small fraction of the volume probed by advanced LIGO/VIRGO. The case with LSST is more promising, with sensitivity in the R-band out to ~ 250 Mpc. Discovery of r -process ejecta in the U or B bands with any facility would appear to be quite difficult, given the heavy line blanketing at these wavelengths.

Given that our models predict that most of the emission is at longer wavelengths, improving detection capabilities in the near infrared may greatly aid in future searches for EM counterparts. Ground based facilities with sensitivity in the I or Y bands ($0.8 - 1.1\mu\text{m}$) may benefit from these capabilities, as the r -process transients are generally ~ 1 magnitude brighter in these bands than in R-band. The construction of space based facilities such as WFIRST (Green et al. 2012) and Euclid (Amendola et al. 2012) would be of particular interest. WFIRST is proposed to have an H-band depth of ~ 25 magnitudes, with Euclid achieving a similar sensitivity. As our fiducial model is much brighter in the infrared ($M_H \simeq -15$) than in the optical bands, such facilities could potentially make a detection out to a distance of ~ 1000 Mpc, encompassing the entire LIGO/VIRGO volume.

Discovering the EM counterparts to NSMs would be made significantly easier if, in addition to r -process elements, these events also separately eject some significant amount of ^{56}Ni or lower mass ($Z < 58$) radioactive isotopes. Our models predict that such “lanthanide-free” light curves are reasonably bright in the optical bands ($M_B \approx M_R \approx -15$) and would be within range for many upcoming optical transient surveys. It is plausible that winds from a post-merger accretion disk may produce such lighter element outflows, although more detailed simulations are needed to constrain the mass and composition of the material ejected. Clearly any detection of a short-lived optical transient should, if possible, be immediately followed up at infrared wavelengths to look for a coincident r -process transient from the tidal tails. Discovery of such a two component light curve and spectrum would be a very strong signature of a NSM. It would also provide insight into the merger and post-merger physics

by separately constraining the mass ejected by different mechanisms.

The work we have presented here is an important step towards improving our predictions of the radioactive transients from NSMs. However, much remains to be done. The opacities we have used, while more realistic than previous estimates, are still subject to important uncertainties. In particular, we need comprehensive structure calculations to derive radiative data for all lanthanides. In addition, more detailed simulations of the dynamics and nucleosynthesis of the mass ejection are needed to better predict the mass, composition, and geometry of the ejecta. Of special interest are the properties of the disk wind and any mixing of these outflows with the tidal tail material. Finally, 3-dimensional radiative transfer calculations will be needed to predict the light curves of multi-component mass ejections and to determine their dependence on viewing angle. Such the-

oretical work should improve our understanding of the EM counterparts to gravitational wave sources, and the heavy elements they produce.

This research has been supported by a Department of Energy Office of Nuclear Physics Early Career Award, and by the Director, Office of Energy Research, Office of High Energy and Nuclear Physics, Divisions of Nuclear Physics, of the U.S. Department of Energy under Contract No. DE-AC02-05CH11231. This work is supported in part by an NSF Division of Astronomical Sciences collaborative research grant AST-1206097. We are grateful for computing time made available the National Energy Research Scientific Computing Center, which is supported by the Office of Science of the U.S. Department of Energy under Contract No. DE-AC02-05CH11231.

REFERENCES

- Abramovici, A., Althouse, W. E., Drever, R. W. P., et al. 1992, *Science*, 256, 325, 325
- Amendola, L., Appleby, S., Bacon, D., et al. 2012, ArXiv e-prints, arXiv:1206.1225
- Arnett, W. D. 1979, *ApJ*, 230, L37, L37
- . 1982, *ApJ*, 253, 785, 785
- Badnell, N. R. 2011, *Computer Phys. Commun.*, 182, 1528, 1528
- Bloom, J. S., Holz, D. E., Hughes, S. A., et al. 2009, ArXiv e-prints, arXiv:0902.1527
- Chevalier, R. A., & Soker, N. 1989, *ApJ*, 341, 867, 867
- Darbha, S., Metzger, B. D., Quataert, E., et al. 2010, *MNRAS*, 409, 846, 846
- Eastman, R. G., & Pinto, P. A. 1993, *ApJ*, 412, 731, 731
- Eichler, D., Livio, M., Piran, T., & Schramm, D. N. 1989, *Nature*, 340, 126, 126
- Freiburghaus, C., Rosswog, S., & Thielemann, F.-K. 1999, *ApJ*, 525, L121, L121
- Goriely, S., Bauswein, A., & Janka, H.-T. 2011, *ApJ*, 738, L32, L32
- Goriely, S., Demetriou, P., Janka, H.-T., Pearson, J. M., & Samyn, M. 2005, *Nuclear Physics A*, 758, 587, 587
- Green, J., Schechter, P., Baltay, C., et al. 2012, ArXiv e-prints, arXiv:1208.4012
- Heiter, U., Barklem, P., Fossati, L., et al. 2008, *Journal of Physics Conference Series*, 130, 012011, 012011
- Hotokezaka, K., Kiuchi, K., Kyutoku, K., et al. 2013, *Phys. Rev. D*, 87, 024001, 024001
- Janka, H.-T., Eberl, T., Ruffert, M., & Fryer, C. L. 1999, *ApJ*, 527, L39, L39
- Karp, A. H., Lasher, G., Chan, K. L., & Salpeter, E. E. 1977, *ApJ*, 214, 161, 161
- Kasen, D., Badnell, N. R., & Barnes, J. 2013, *ApJ* submitted
- Kasen, D., Thomas, R. C., & Nugent, P. 2006, *ApJ*, 651, 366, 366
- Kurucz, R., & Bell, B. 1995, *Atomic Line Data* (R.L. Kurucz and B. Bell) Kurucz CD-ROM No. 23. Cambridge, Mass.: Smithsonian Astrophysical Observatory, 1995., 23
- Lattimer, J. M., & Schramm, D. N. 1974, *ApJ*, 192, L145, L145
- . 1976, *ApJ*, 210, 549, 549
- Law, N. M., Kulkarni, S. R., Dekany, R. G., et al. 2009, 121, 1395, 1395
- Lee, W. H. 2001, *MNRAS*, 328, 583, 583
- Li, L.-X., & Paczyński, B. 1998, *ApJ*, 507, L59, L59
- LSST Science Collaborations. 2009, arXiv:0912.0201
- Metzger, B. D., & Berger, E. 2012, *ApJ*, 746, 48, 48
- Metzger, B. D., Piro, A. L., & Quataert, E. 2008, *MNRAS*, 390, 781, 781
- Metzger, B. D., Martínez-Pinedo, G., Darbha, S., et al. 2010, *MNRAS*, 406, 2650, 2650
- Narayan, R., Paczynski, B., & Piran, T. 1992, *ApJ*, 395, L83, L83
- Nissanke, S., Kasliwal, M., & Georgieva, A. 2012, ArXiv e-prints, arXiv:1210.6362
- Oechslin, R., Janka, H.-T., & Marek, A. 2007, *A&A*, 467, 395, 395
- Paczynski, B. 1986, *ApJ*, 308, L43, L43
- Pinto, P. A., & Eastman, R. G. 2000, *ApJ*, 530, 757, 757
- Roberts, L. F., Kasen, D., Lee, W. H., & Ramirez-Ruiz, E. 2011, *ApJ*, 736, L21, L21
- Rosswog, S. 2005, *ApJ*, 634, 1202, 1202
- Rosswog, S., Davies, M. B., Thielemann, F.-K., & Piran, T. 2000, *A&A*, 360, 171, 171
- Rosswog, S., Liebendörfer, M., Thielemann, F.-K., et al. 1999, *A&A*, 341, 499, 499
- Rosswog, S., Thielemann, F. K., Davies, M. B., Benz, W., & Piran, T. 1998, in *Nuclear Astrophysics*, ed. W. Hillebrandt & E. Müller, 103
- Schutz, B. F. 1986, *Nature*, 323, 310, 310
- Schutz, B. F. 2002, in *Lighthouses of the Universe: The Most Luminous Celestial Objects and Their Use for Cosmology*, ed. M. Gilfanov, R. Sunyaev, & E. Churazov, 207
- Sobolev, V. V. 1960,
- Stubbs, C. W. 2008, *Classical and Quantum Gravity*, 25, 184033, 184033
- Surman, R., McLaughlin, G. C., & Hix, W. R. 2006, *ApJ*, 643, 1057, 1057
- Surman, R., McLaughlin, G. C., Ruffert, M., Janka, H.-T., & Hix, W. R. 2008, *ApJ*, 679, L117, L117